

Structure and Properties of Mixed-Chain Phosphatidylcholine Bilayers[†]

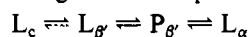
Jyotsna Shah, P. K. Sripada, and G. Graham Shipley*

Departments of Biophysics and Biochemistry, Boston University School of Medicine, Housman Medical Research Center, Boston, Massachusetts 02118

Received December 1, 1989; Revised Manuscript Received January 16, 1990

ABSTRACT: The structural and thermotropic properties of the hydrated mixed-chain phosphatidylcholines (PCs), C(8):C(18)-PC and C(10):C(18)-PC, have been studied by X-ray diffraction and differential scanning calorimetry. For fully hydrated C(8):C(18)-PC, the reversible chain melting transition is observed at 9.9 °C ($\Delta H = 7.3$ kcal/mol). X-ray diffraction at 0 °C (below the chain melting transition) shows a small bilayer repeat distance, $d = 51.0$ Å, and a sharp, symmetric wide-angle reflection at 4.1 Å, characteristic of a mixed interdigitated bilayer gel phase [see McIntosh, T. J., Simon, S. A., Ellington, J. C., Jr., & Porter, N. A. (1984) *Biochemistry* 23, 4038-4044; Hui, S. W., Mason, J. T., & Huang, C. (1984) *Biochemistry* 23, 5570-5577]. At 30 °C (above the chain melting transition), a diffuse band is observed at 4.5 Å characteristic of an L_α phase but with an increased bilayer periodicity, $d = 61$ Å. Both the calculated lipid bilayer thickness (d_l) and that determined directly from electron density profiles (d_{p-p}) show unusual increases as a consequence of chain melting. In contrast, fully hydrated C(10):C(18)-PC shows an asymmetric endothermic transition at 11.8 °C. Below the chain melting transition, two lamellar phases are present, corresponding to coexisting interdigitated ($d = 52.3$ Å) and noninterdigitated ($d = 62.5$ Å) bilayer gel phases. The relative amounts of these phases depend upon the low-temperature incubation and/or hydration conditions, suggesting conversions, albeit kinetically complex, between metastable, and stable phases. The different behavior of C(8):C(18)-PC and C(10):C(18)-PC, as well as their positional isomers, is rationalized in terms of the molecular conformation of PC.

Biological membranes contain a heterogeneous mixture of phospholipids differing from each other with respect to their head-group structure, hydrocarbon chain length at the *sn*-1 and *sn*-2 positions of the glycerol backbone, degree of unsaturation of the acyl chains, and mode of attachment of the hydrocarbon chains to the glycerol moiety. Due to this complex lipid composition, it is extremely difficult to ascertain the physical properties and functional roles of individual lipids in intact membranes. Model systems consisting of either natural or synthetic phospholipids have been a valuable tool in obtaining basic information on membrane phospholipids, and various studies have been performed on hydrated bilayer systems of phosphatidylcholines (PCs),¹ phosphatidylethanolamines, etc. For PCs, most of the previous studies have focused on symmetric lipids with identical saturated chains at the *sn*-1 and *sn*-2 positions, e.g., C(18):C(18)-, C(16):C(16)-, and C(14):C(14)-PC, and on the basis of calorimetric, X-ray diffraction, and spectroscopic studies, it was proposed that these molecules pack "independently" to form the two monolayer halves of a bilayer (Chapman et al., 1967; Mabrey & Sturtevant, 1976; Gaber & Peticolas, 1977; Yellin & Levin, 1977; Janiak et al., 1976, 1979; Barenholz & Thompson, 1980; Ruocco & Shipley, 1982a,b). A general scheme is proposed for the structural changes with temperature:



where L_c denotes the crystalline phase, L_g the gel phase, P_g the rippled gel phase, and L_α the liquid-crystalline phase [see, for example, Tardieu et al. (1973) and Ruocco and Shipley (1982a,b)].

However, a modification to this general picture was required to describe the behavior of mixed-chain PCs with different

fatty acids ester-linked at the *sn*-1 and *sn*-2 positions (Mason et al., 1981a; Chen & Sturtevant 1981; Huang et al., 1983; Serrallach et al., 1984; Stumpel et al., 1981, 1983; McIntosh et al., 1984; Hui et al., 1984; Boggs & Mason, 1986; Mattai et al., 1987). For the hydrated mixed-chain PC bilayers, the transition entropies (Mason et al., 1981a) and the change of Raman spectral indices (monitoring chain all-trans:gauche states) in the C-C and C-H stretching mode regions (Huang et al., 1983) conform to a smooth hyperbolic curve and vary in the order of C(18):C(18)- > C(18):C(16)- > C(18):C(14)- < C(18):C(12)- < C(18):C(10)-PC. Clearly, there is minimum in the extent of chain disordering occurring at the gel-liquid-crystalline phase transition for C(18):C(14)-PC bilayers. The calorimetric data for these mixed-chain PCs were rationalized by proposing that the bilayer gel state transforms from one where the two monolayer leaflets are discrete [C(18):C(18)- and C(18):C(16)-PC] to one where they are just beginning to interdigitate [C(18):C(14)-PC]. The gel state of the C(18):C(14)-PC bilayer is proposed to be strongly disordered toward the methyl ends as a consequence of the close proximity of sterically large terminal methyl groups forming the slightly interdigitated bilayer (Mason et al., 1981a).

However, the more asymmetric PCs C(18):C(12)- and C(18):C(10)-PC were shown to have a more ordered packing than C(18):C(14)-PC, and on the basis of structural studies, it was established that these PCs form mixed interdigitated bilayers in the gel state (McIntosh et al., 1984; Hui et al., 1984). In this packing model, the long *sn*-1 acyl chain extends fully across the entire width of the bilayer, and the short *sn*-2 chain packs end-to-end with a short chain of another PC molecule from the opposite leaflet of the bilayer. Thus, there

[†] Supported by National Institutes of Health Grant HL-26335.

* Address correspondence to this author at the Department of Biophysics, Boston University School of Medicine.

¹ Abbreviations: PC, phosphatidylcholine; DSC, differential scanning calorimetry.

are three hydrocarbon chains per lipid head group, with calculations of PC and chain areas supporting this "triple-chain" concept. Calculation of rotameric energies (McIntosh et al., 1984) showed that this phase (L_{β}) is energetically favorable for mixed-chain PCs provided that the chain length difference between *sn*-1 and *sn*-2 acyl chains (ΔC) is approximately half of the length of the longer acyl chain (CL) using the nomenclature of Mason et al. (1981a). Recently, Xu & Huang (1987) examined a series of asymmetric PCs with the ratio of $\Delta C/CL$ approximately 0.5 [e.g., C(16):C(9)-, C(16):C(10)-, C(18):C(11)-, C(20):C(11)-, C(20):C(12)-, C(22):C(12)-, C(8):C(18)-, C(10):C(22)-PC, etc.], and on the basis of their thermotropic phase behavior, it was concluded that different asymmetric PCs, sharing the same characteristic $\Delta C/CL \approx 0.5$, indeed self-assemble to form mixed interdigitated bilayers in the gel phase.

In our earlier publication (Mattai et al., 1987), it was shown that the chain melting transition temperatures (T_m) and enthalpies (ΔH) show a decreasing trend in going from C-(18):C(18)-PC to C(18):C(14)-PC and then slightly increase for C(18):C(12)-PC and C(18):C(10)-PC. Similar behavior was shown by the other series of mixed-chain PCs with systematic variation at the *sn*-1 position [i.e., a decrease from C(18):C(18)-PC to C(12):C(18)-PC and then a slight increase for C(10):C(18)-PC]. In the present investigation, we have extended our calorimetric studies of the two series, focusing on C(18):C(12)-, C(18):C(10)-, C(18):C(8)-, C(18):C(6)-, C(18):C(4)-, and C(18):C(2)-PC, as well as on C(12):C(18)-, C(10):C(18)-, C(8):C(18)-, and C(6):C(18)-PC. In addition, to test whether asymmetric mixed-chain PCs with the longer fatty acyl chain at the *sn*-2 position exhibit structural and thermotropic properties similar to those of C(18):C(12)-PC ($\Delta C/CL = 0.44$) and C(18):C(10)-PC ($\Delta C/CL = 0.56$), we undertook a detailed structural and thermotropic study of C(8):C(18)-PC ($\Delta C/CL = 0.55$) and C(10):C(18)-PC ($\Delta C/CL = 0.42$) as a function of hydration using X-ray diffraction and differential scanning calorimetry (DSC). These PCs had not been studied by X-ray diffraction, but on the basis of the thermodynamic data, it has been predicted that at full hydration these lipids form a mixed interdigitated gel phase (Mason et al., 1981a). In the present study, we found that hydrated C(8):C(18)-PC forms a gel-state bilayer at $T < T_m$, the chain-melting temperature, with a very small bilayer thickness consistent with the interdigitated triple-chain structure and which does not change significantly with hydration. However, hydrated C(10):C(18)-PC exhibited coexistence of two phases at $T < T_m$, whereas at $T > T_m$ only a single bilayer phase occurred.

MATERIALS AND METHODS

C(18):C(18)-PC was obtained in lyophilized form (99% purity) from Avanti Polar Lipids (Birmingham, AL). Purity was checked by thin-layer chromatography using the solvent system $\text{CHCl}_3/\text{CH}_3\text{OH}/\text{H}_2\text{O}$ (65:25:4 v/v) and $\text{CHCl}_3/\text{CH}_3\text{OH}/\text{NH}_4\text{OH}$ (65:25:4). Rexyn-I-300 was obtained from Fisher Scientific, Fair Lawn, NJ, and Unisil silicic acid 100–200 mesh was from Clarkson Chemical Co., Williamsport, PA. The mixed-chain PCs were synthesized according to the procedures of both Gupta et al. (1977) and Mason et al. (1981b) using the corresponding lysophosphatidylcholines (Avanti Polar Lipids, Birmingham, AL) and fatty acid anhydrides (Nu Chek Prep, Elysian, MN). The isomeric purity of these lipids was checked by phospholipase A_2 cleavage of the fatty acid at the *sn*-2 position of the glycerol backbone, followed by gas-liquid chromatography analysis of the methyl esters of the acids according to Morrison and Smith (1964).

Acyl chain migration of <5% was observed.

Differential Scanning Calorimetry (DSC). Hydrated multilamellar suspensions were prepared by adding distilled, deionized water directly, using a Hamilton syringe, to stainless-steel DSC pans containing known amounts of mixed-chain PCs. After the DSC pans were sealed, proper mixing was ensured by heating and cooling the sample to temperatures above and below the main transition temperature of the lipid several times. Samples were stored at -4°C .

Calorimetric measurements [T_m , degrees centigrade ($\pm 0.2^\circ\text{C}$); ΔH , kilocalories per mole ($\pm 0.3 \text{ kcal/mol}$)] were made with a Perkin-Elmer (Norwalk, CT) DSC-2 differential scanning calorimeter at a heating and cooling rate of $5^\circ\text{C}/\text{min}$. Data were analyzed by using a Perkin-Elmer thermal analysis data station (Model 3500), and transition enthalpies were calibrated by comparison with the gallium standard.

X-ray Diffraction. Hydrated samples were prepared by adding a weighed amount of PC into a thin-walled (1.0-mm diameter) quartz capillary, followed by centrifugation to ensure that the lipid reached the bottom of the capillary. Distilled, deionized water was added to the capillary and the tube re-centrifuged, weighed, and then flame-sealed using a propane-oxygen flame. To obtain homogeneous mixing, the sample was heated and cooled to temperatures above and below the transition temperature of the PC and stored at -4°C until use.

X-ray diffraction patterns were recorded with photographic film using nickel-filtered $\text{Cu K}\alpha$ radiation ($\lambda = 1.5418 \text{ \AA}$) from an Elliott GX-6 rotating anode generator (Elliott Automation, Borehamwood, U.K.). The X-rays were focused into a point source using cameras with toroidal and double-mirror optics. The intensities of the diffraction lines were measured by using an Automatic Recording Microdensitometer, Model MK III C. (Joyce-Loebl Ltd., Gateshead, England).

Starting with the bilayer periodicity [d , angstroms ($\pm 0.25 \text{ \AA}$)], the values of lipid bilayer thickness (d_l), water layer thickness (d_f), and area (S) available to one lipid molecule were calculated by using the formulas (Luzzati, 1968):

$$d_l = d[1 + (\nu_f/\nu_l)(1 - C)/C]^{-1}$$

$$d_f = d - d_l$$

$$S = 2M_r\nu_l/d_l(N \times 10^{-24})$$

where ν_f and ν_l are the partial specific volumes of water and lipid, respectively, C is the lipid concentration, M_r is the molecular weight of the lipid, and N is Avogadro's number. At present, ν_l values for mixed-chain PCs either at full hydration or at lower hydrations are not available. Thus, we have used values [calculated by using the approach adopted by Tardieu et al. (1973)] of 0.935 mL/g for the gel state and 1.00 mL/g for the liquid-crystalline state. Similar values of ν_l were used by McIntosh et al. (1984) in their study of C(18):C(10)-PC. These values of ν_l are in good agreement with those determined by dilatometry for a series of saturated chain PCs in the gel and liquid-crystalline states (Nagle & Wilkinson, 1978). The value of ν_f is assumed to be 1.0 mL/g .

In order to calculate electron density profiles, the observed lamellar intensities, $I(h)$, were corrected for the Lorentz factor (in our geometry and for unoriented samples this is $\propto h^2$) giving $h^2I(h)$, and each hydration set was normalized with respect to each other by using the procedure described by Worthington and Blaurock (1969), i.e.

$$(2/d)\sum h^2I(h) = \text{constant}$$

The corresponding scaled, normalized structure amplitudes, $F(h)$, are plotted as a function of the reciprocal coordinate s

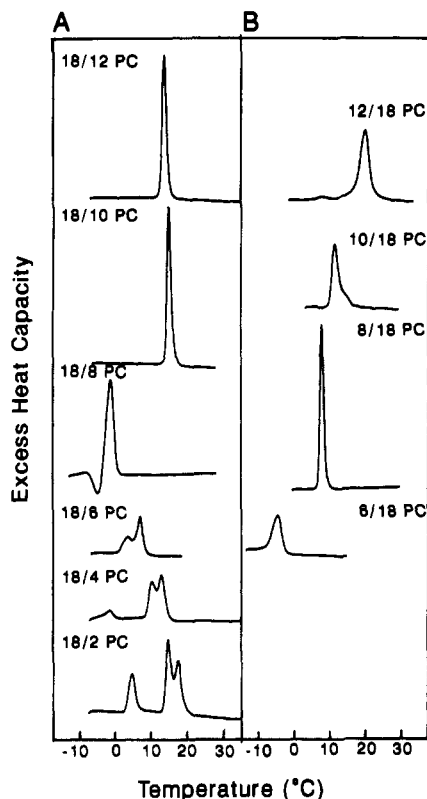


FIGURE 1: DSC heating scans of 80% hydrated mixed-chain PCs. (A) C(18):C(*n*)-PC series and (B) C(*n*):C(18)-PC series. Heating rates, 5 °C/min.

($s = 2 \sin \theta/\lambda$). Phasing of the lamellar reflections is done by inspection of the plotted amplitude data and by use of the Shannon sampling theorem (Shannon, 1949). For the latter, first $F(0)$ was determined by using the method described by King (1971) and King and Worthington (1971), and the continuous amplitudes were calculated for all phase combinations. The phase combination providing a satisfactory fit to all hydration amplitudes is selected.

RESULTS

Calorimetric Properties of Mixed-Chain PCs. C(18):C(18)-, C(18):C(16)-, C(16):C(18)-, C(18):C(14)-, and C(14):C(18)-PC have been studied in detail by previous workers (Chapman et al., 1967; Mabrey & Sturtevant, 1976; Stumpel et al., 1981, 1983). We have extended our own calorimetric studies (Mattai et al., 1987) using C(18):C(12)-, C(18):C(10)-, C(18):C(8)-, C(18):C(6)-, C(18):C(4)-, and C(18):C(2)-PC as well as C(12):C(18)-, C(10):C(18)-, C(8):C(18)-, and C(6):C(18)-PC. It has been observed previously that the thermotropic properties of both the C(18):C(*n*)-PC and C(*n*):C(18)-PC series do not change continuously as the chain length asymmetry is increased (Huang & Mason, 1986; Mattai et al., 1987). DSC heating and cooling scans of the lower homologues of the two PC series were recorded, and their heating scans are shown in Figure 1. In the C(18):C(*n*)-PC series (where *n* varies from 12 to 2), the first two members (*n* = 12 and 10) showed a single sharp endothermic transition whereas the other four (*n* = 8, 6, 4, 2) exhibited more complex thermotropic behavior (Figure 1A). C(18):C(12)-PC and C(18):C(10)-PC show reversible thermal transitions at 15.9 and 17.0 °C with transition enthalpies of 7.4 and 7.9 kcal/mol, respectively. However, on heating, C(18):C(8)-PC shows an exothermic transition at -3.4 °C ($\Delta H = 1.6$ kcal/mol) followed by an endothermic transition at 0.2 °C ($\Delta H = 6.2$ kcal/mol).² On cooling (data not shown), an exothermic

transition is observed at -7.9 °C ($\Delta H = 2.3$ kcal/mol). The other three members of the series show multiple transitions on heating. C(18):C(6)-PC shows an endothermic transition at 8.2 °C with a pronounced shoulder at 4.6 °C (combined $\Delta H = 3.6$ kcal/mol). On cooling, a single exothermic transition is observed at -1.1 °C ($\Delta H = 3.9$ kcal/mol). For C(18):C(4)-PC, three transitions are observed at -0.5 °C ($\Delta H = 0.5$ kcal/mol), 11.4 °C, and 14.0 °C (combined $\Delta H = 4.0$ kcal/mol). The cooling scan shows two transitions at 7.0 °C ($\Delta H = 4.2$ kcal/mol) and -7.2 °C ($\Delta H = 0.4$ kcal/mol). The final member of this series, C(18):C(2)-PC, also displays three endothermic transitions at 5.7 °C ($\Delta H = 1.6$ kcal/mol), 15.8 °C, and 18.5 °C (combined $\Delta H = 5.0$ kcal/mol). The corresponding exotherm occurred at 11.6 °C on cooling with a significantly reduced enthalpy ($\Delta H = 0.1$ kcal/mol), presumably due to the slow kinetics of a micelle \rightarrow bilayer transition (Huang & Mason, 1986; Mattai & Shipley, 1986).

The members of the C(*n*):C(18)-PC series show a simpler pattern of behavior (Figure 1B). On heating, C(12):C(18)-PC exhibits two transitions, a small endotherm at 8.9 °C ($\Delta H = 0.3$ kcal/mol) and the main transition at 21.2 °C ($\Delta H = 6.4$ kcal/mol). On cooling (data not shown), two corresponding exotherms are observed at 5.2 °C ($\Delta H = 0.2$ kcal/mol) and 17.7 °C ($\Delta H = 5.0$ kcal/mol). For C(10):C(18)-PC, the heating curve shows a single, albeit asymmetric, transition at 11.8 °C ($\Delta H = 6.3$ kcal/mol) with a high-temperature shoulder. The corresponding exothermic transition is observed at 8.5 °C ($\Delta H = 6.3$ kcal/mol) on cooling. The next member of the series, C(8):C(18)-PC, gives a sharp, symmetric transition at 9.9 °C ($\Delta H = 7.3$ kcal/mol) on heating, with a corresponding exothermic transition at 4.4 °C ($\Delta H = 7.3$ kcal/mol) on cooling. The final member of this series, C(6):C(18)-PC, also displayed a single transition both on heating ($T_m = 5.2$ °C, $\Delta H = 1.8$ kcal/mol) and on cooling ($T_m = -14.1$ °C).

The chain melting transition temperatures (T_m) and corresponding enthalpies (ΔH_m) were determined from the second heating curves in order to avoid any complications due to low-temperature metastable behavior. Figure 2 depicts the behavior of T_m and ΔH_m with varying *sn*-1 and *sn*-2 chain length and includes previously published data from Mattai et al. (1987) for the higher members of the two series. For the C(18):C(*n*)-PC series (Figure 2A, right), T_m decreases from 55.5 to 15.9 °C as *n* decreases from 18 to 12. However, for C(18):C(10)-PC, T_m increases slightly (17.0 °C) and then decreases again sharply for the next member of the series, C(18):C(8)-PC ($T_m = 0.3$ °C). On further decreasing the chain length, T_m (assumed to be the highest temperature transition) increases progressively to 8.2 °C for C(18):C(6)-PC, 14.0 °C for C(18):C(4)-PC, and 18.5 °C for C(18):C(2)-PC. For the C(*n*):C(18)-PC series (Figure 2A, left), T_m is reduced sharply from 55.5 to 11.8 °C as *n* decreases from 18 to 10. For C(8):C(18)-PC, there is just a slight decrease in T_m (to 9.9 °C) followed by a large decrease for C(6):C(18)-PC ($T_m = -5.2$ °C).

A similar pattern of behavior was shown by the transition enthalpy (Figure 2B) and entropy (data not shown). ΔH_m decreases as the *sn*-2 chain length decreases from 18 ($\Delta H = 10.6$ kcal/mol) to 14 (5.5 kcal/mol) and increases again for

² Although we have not performed a detailed study of C(18):C(8)-PC, we have shown that if the sample is heated through the exotherm to -2 °C, immediately cooled to -12 °C, and then reheated, the exotherm is not observed; only the main endotherm at 0.2 °C with the same transition enthalpy as determined in the initial heating run is observed. This implies the presence of low-temperature metastable gel forms of C(18):C(8)-PC.

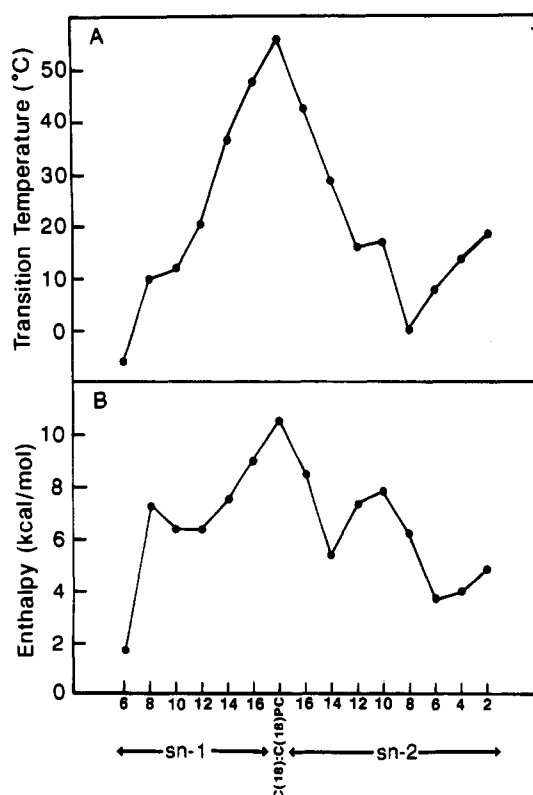


FIGURE 2: Dependence of transition temperatures (A) and transition enthalpies (B) as a function of acyl chain length variation in the *sn*-1 and *sn*-2 positions of the glycerol backbone. (Data are derived from the second heating scans.) Values for C(18):C(18)-, C(18):C(16)-, C(18):C(14)-, C(16):C(18)-, and C(14):C(18)-PC are taken from Mattai et al. (1987).

C(18):C(12)-PC ($\Delta H = 7.4$ kcal/mol) and C(18):C(10)-PC (7.9 kcal/mol), followed by a decrease in ΔH_m for the next two members of the series [6.3 kcal/mol for C(18):C(8)-PC and 3.6 kcal/mol for C(18):C(6)-PC]. ΔH increases again for C(18):C(4)-PC (4.0 kcal/mol) and C(18):C(2)-PC (5.0 kcal/mol). It should be noted that a combined enthalpy for the two higher temperature transitions was calculated for C(18):C(6)-, C(18):C(4)-, and C(18):C(2)-PC (see Figure 1A). For the C(*n*):C(18)-PC series, ΔH_m decreases with decreasing *sn*-1 chain length from *n* = 18 to 12, increases slightly for C(10):C(18)-PC (6.3 kcal/mol) and C(8):C(18)-PC (7.3 kcal/mol), and then decreases sharply for C(6):C(18)-PC (1.7 kcal/mol). Thus, the dependence of both T_m and ΔH_m on chain length shows a discontinuity on both sides of the "parent" molecule C(18):C(18)-PC (see Figure 2A,B) indicative of structural alterations. Here, we focus on the behavior of two members of the C(*n*):C(18)-PC series in the region of this discontinuity, C(8):C(18)-PC and C(10):C(18)-PC.

Calorimetric Properties of C(8):C(18)-PC and C(10):C(18)-PC. Fully hydrated (80 wt % water) samples of C(8):C(18)- and C(10):C(18)-PC were stored for 2 weeks at -10°C prior to transfer to the scanning calorimeter. In Figure 3, DSC heating curves are presented for C(8):C(18)-PC and C(10):C(18)-PC after low-temperature incubation. C(8):C(18)-PC displays a sharp, symmetric transition at 9.9°C ($\Delta H = 7.2$ kcal/mol) as shown in Figure 3A (top). On cooling, an exothermic transition is observed at 4.4°C ($\Delta H = 7.3$ kcal/mol) with a high-temperature shoulder (Figure 3A, middle). On immediate reheating, an identical endothermic transition is observed (Figure 3A, bottom), indicating completely reversible behavior. For C(10):C(18)-PC, a single

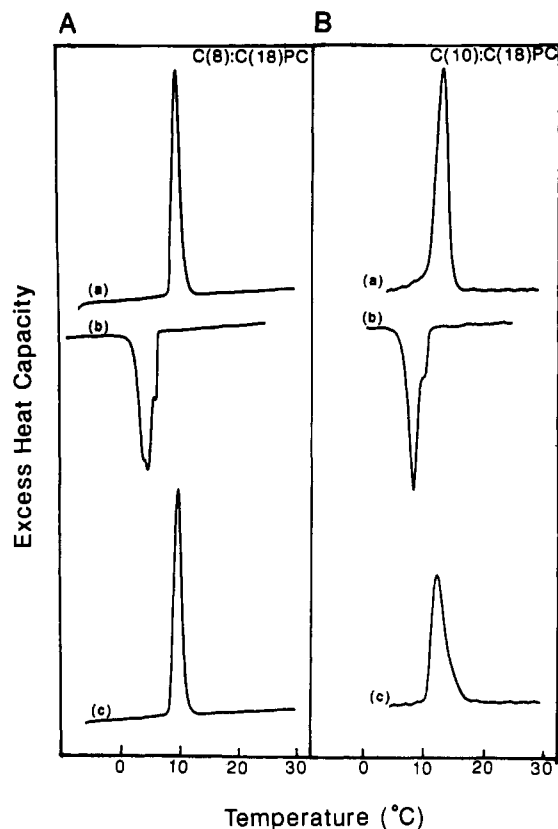


FIGURE 3: DSC heating scans of C(8):C(18)-PC (A) and C(10):C(18)-PC (B), following low-temperature incubation at -4°C . First heating scans (top); cooling scans (middle); immediate reheating scans (bottom). Heating/cooling rates, $5^\circ\text{C}/\text{min}$.

broad transition is observed at 13.7°C ($\Delta H = 9.3$ kcal/mol) as shown in Figure 3B (top). On cooling (Figure 3B, middle), an exothermic transition is observed at 8.5°C with a small high-temperature shoulder, but with a significantly lower enthalpy ($\Delta H = 6.3$ kcal/mol). Immediate reheating (Figure 3B, bottom) shows an asymmetric endothermic transition at 11.8°C with significantly reduced enthalpy ($\Delta H = 6.3$ kcal/mol) compared to that observed on the initial heating run after low-temperature incubation (cf. Figure 3B, top and bottom). Thus, a comparison of Figure 3A and Figure 3B reveals that C(8):C(18)-PC shows a completely reversible thermal transition whereas C(10):C(18)-PC exhibits an irreversible transition at 13.7°C after low-temperature incubation, suggesting the formation of a more ordered low-temperature phase (Ruocco & Shipley, 1982a,b; Mattai et al., 1987).

The heating scans of C(8):C(18)-PC and C(10):C(18)-PC at different hydrations (without low-temperature equilibration) are shown in panels A and B, respectively, of Figure 4. For C(8):C(18)-PC, a single symmetric endothermic transition is observed at all hydrations, with the transition temperature decreasing progressively from 11.1°C (20 wt % water) to 9.9°C (60 wt % water) with increasing hydration (Figure 4A). However, on cooling, the exothermic transition shows some asymmetry above 30% water content which increases with increasing hydration (data not shown, but see Figure 3A, middle). C(10):C(18)-PC (Figure 4B) shows more complex hydration behavior compared to C(8):C(18)-PC, particularly at low water contents. At 10 wt % water, a broad exothermic transition at -2.8°C ($\Delta H = 3.7$ kcal/mol) is followed by two endothermic transitions at 15.8 and 21.5°C (combined enthalpy $\Delta H = 12.0$ kcal/mol). On increasing the hydration, the exothermic transition becomes weaker and disappears at $>30\%$ hydration. The two endothermic transitions decrease

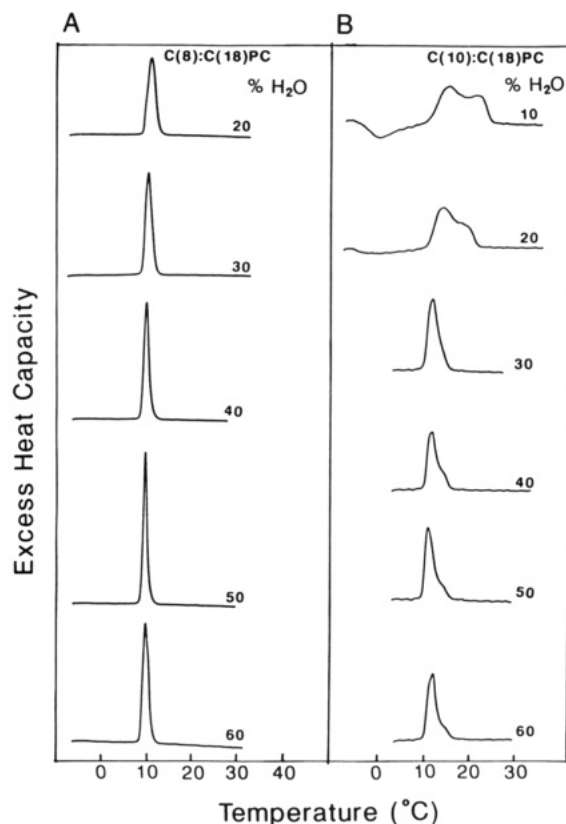


FIGURE 4: Representative DSC heating scans of hydrated C(8):C(18)-PC in the range 20–60 wt % water (A) and C(10):C(18)-PC in the range 10–60 wt % water (B). Heating rates, 5 °C/min.

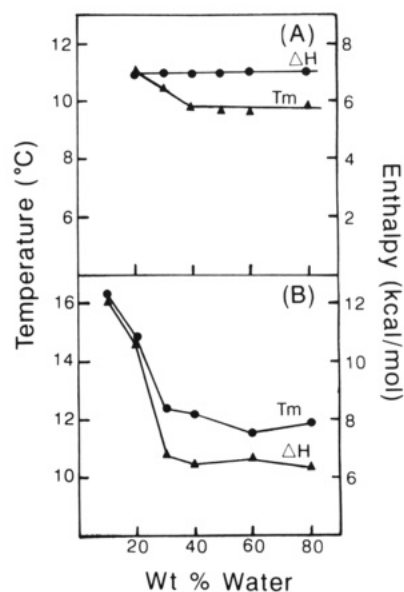


FIGURE 5: Variation of transition temperature (T_m) and enthalpy (ΔH) with water concentration for C(8):C(18)-PC (A) and C(10):C(18)-PC (B).

in temperature with increasing water content, reaching a limiting transition temperature of 11.8 °C. A small shoulder is still apparent on the high-temperature side. The corresponding cooling curves show only single but asymmetric transitions (data not shown, but see Figure 3B, middle).

The transition temperature (T_m) and enthalpy (ΔH_m) for C(8):C(18)-PC and C(10):C(18)-PC are plotted as a function of water content in Figure 5. For C(8):C(18)-PC (Figure 5A), T_m decreases progressively from 11.1 to 9.9 °C on increasing hydration with no change in T_m at >40 wt % water.

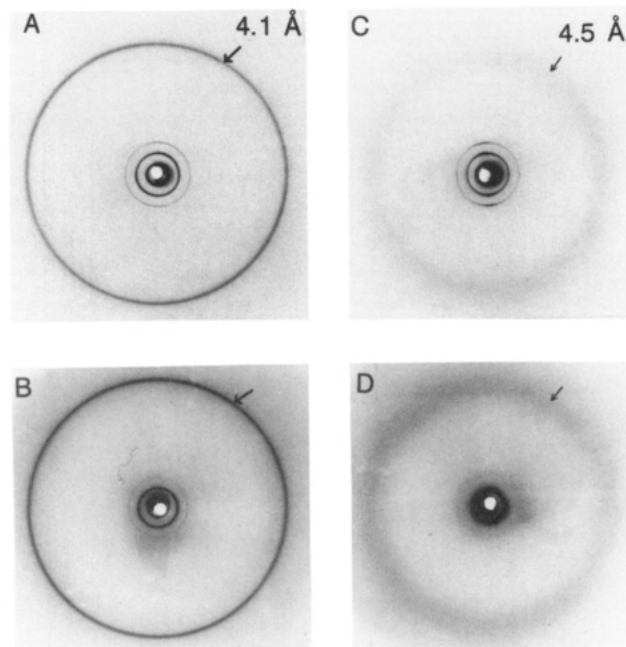


FIGURE 6: X-ray diffraction patterns of C(8):C(18)-PC: 20% H₂O at 0 °C (A); 60% H₂O at 0 °C (B); 20% H₂O at 30 °C (C); 60% H₂O at 30 °C (D).

Over this hydration range, there is no significant change in transition enthalpy (Figure 5A). For C(10):C(18)-PC (Figure 5B), T_m decreases from 16.3 to 11.8 °C with increasing water content from 10% to 40% and levels off at approximately 40% water content. ΔH_m , in contrast to C(8):C(18)-PC, also decreases from 12.1 to 6.3 kcal/mol on increasing the hydration from 10% to 40% water, remaining constant thereafter (Figure 5B).

X-ray Diffraction Studies of C(8):C(18)- and C(10):C(18)-PC. The structures of various phases are characterized by using X-ray diffraction. C(8):C(18)-PC was studied as a function of hydration below (0 °C) and above (30 °C) the chain melting transition (T_m). The low-angle reflections are typical of lamellar phases, both at low and at high temperatures for all hydrations (for example, see Figure 6). At $T < T_m$, for C(8):C(18)-PC at 20 wt % water (Figure 6A), a single sharp, symmetric wide-angle reflection at 4.1 Å (arrowed) is observed together with a series of lamellar reflections ($h = 1-5$) corresponding to a bilayer periodicity $d = 46.0$ Å. The sharp reflection at 4.1 Å, indicative of a gel state with hexagonally packed chains, is present at all hydrations, for example, 60% H₂O (Figure 6B); however, the bilayer repeat distance increases with hydration, to 51.0 Å at 60% water (Figure 6B). At 30 °C ($T > T_m$), a single diffuse wide-angle reflection is observed at 4.5 Å (arrowed) plus a series of lamellar reflections characteristic of the bilayer liquid-crystalline state (L_α) (see Figure 6C,D). The bilayer repeat distance increases from 47.2 to 61.0 Å as the hydration increases from 20 to 60 wt % H₂O (see Figure 6C,D).

The bilayer periodicity d for C(8):C(18)-PC bilayers at 0 °C ($T < T_m$) and 30 °C ($T > T_m$) is plotted as a function of water content as shown in Figure 7. At 0 °C, d increases from 39.7 Å (10% water) to 51.0 Å (40% water) (Figure 7A) and from 43.0 Å (10% water) to 61.0 Å (40% water) at 30 °C (Figure 7B) with no change observed on further increasing the water content. The corresponding calculated values (using the Luzzati formalism, see Materials and Methods) of d_l , d_f , and S are plotted as a function of hydration (Figure 7). At 0 °C, over the hydration range 10–40% water, d_l decreases from 35.5 to 29.8 Å, d_f increases from 4.2 to 21.2 Å, and S

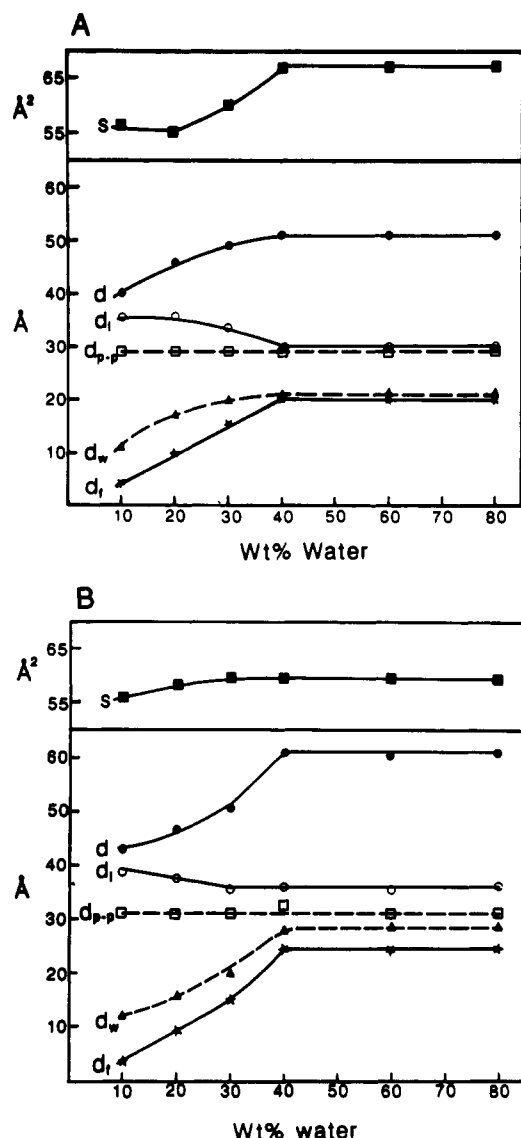


FIGURE 7: Bilayer structural parameters of C(8):C(18)-PC as a function of water content at 0 °C (A) and 30 °C (B). (●) Bilayer periodicity d ; (○) bilayer thickness d_l ; (▲) water thickness d_w ; (■) surface area per C(8):C(18)-PC molecule at the lipid-water interface, calculated by the Luzzati formalism; (□) phosphate to phosphate distance d_{p-p} ; (▲) water layer thickness determined from electron density profiles. Note that the values of d_l , d_w , and S for hydrations >40 wt % water are calculated by assuming a hydration value corresponding to the hydration limit (40 wt % water).

increases from 56.7 to 67.6 \AA^2 (Figure 7A). At 30 °C, over the hydration range 10–40% d_l decreases slightly from 38.7 to 36.6 \AA , d_l increases from 4.3 to 24.4 \AA , and S increases from 55.7 to 58.9 \AA^2 (Figure 7B). For the gel state at 0 °C, the area per hydrocarbon chain, Σ , was also calculated from the wide-angle spacing, $d_s = 4.1$ \AA , by the formula $\Sigma = 2d_s^2/3^{1/2} = 19.5$ \AA^2 [see Tardieu et al. (1973)]. The ratio of the area per molecule to area per hydrocarbon chain is approximately 3:1 for all hydrations studied.

In order to determine the electron density profiles for C(8):C(18)-PC at different hydrations, swelling experiments were carried out at 0 and 30 °C as indicated above. For the gel phase at 0 °C, Figure 8 shows the structure factor amplitudes, $F(s)$, plotted versus the reciprocal coordinate s [$s = 2 \sin \theta / \lambda$] for the lamellar reflections recorded at 10, 20, 30, and 40% hydration. After determination of $F(0)$ (see Materials and Methods), the Shannon sampling theorem (Shannon, 1949; Sayre, 1952; King & Worthington, 1971; Torbet &

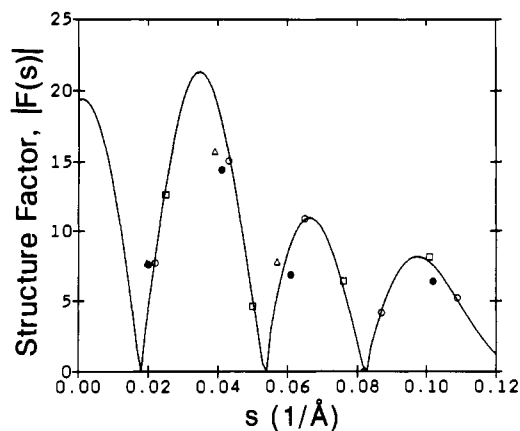


FIGURE 8: Structure amplitudes of C(8):C(18)-PC bilayers at 0 °C at different hydrations. (□) 10% H₂O; (○) 20% H₂O; (●) 30% H₂O; (Δ) 40% H₂O. Continuous line is theoretical curve calculated by using Shannon sampling theory for the data of 20% H₂O (see text).

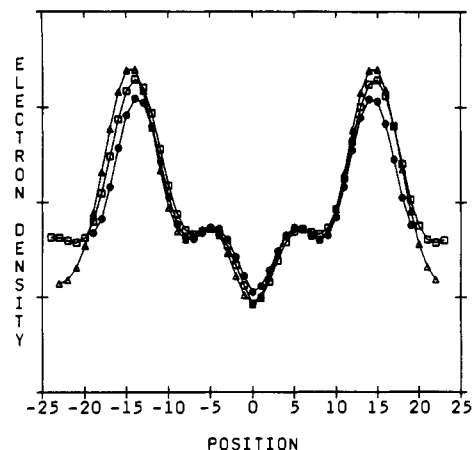


FIGURE 9: Electron density profiles of C(8):C(18)-PC at 0 °C for different hydrations: (●) 10% H₂O ($h = 1-4$); (Δ) 20% H₂O ($h = 1-5$); (□) 30% H₂O ($h = 1-5$). Assigned phases are --+--.

Wilkins, 1976) was used to determine the correct phase combination for all hydration sets. The curve shown for the 20% hydration amplitudes identifies the nodes at $s = 0.017$, 0.054, and 0.082 \AA^{-1} where a change in phase angle (0 or π) could occur and the amplitudes thus phased. The electron density profiles were calculated on the basis of these phases (Figure 9). The profiles indicate a "bilayer" structure with the electron-dense peaks at ± 14.5 \AA corresponding to the phosphorylcholine head groups. At 0 °C, the head-group separation, d_{p-p} , across the bilayer remains constant at 29 \AA , at all hydrations (Figures 7A and 9). The interlayer peak separation provides an additional measure of the water layer thickness, $d_w = d - d_{p-p}$; d_w increases from 11 \AA (10% water) to 20.5 \AA (40% water) (see Figure 7A). A trough is clearly observed at $X = 0$ \AA corresponding to the layer center.

A similar approach was used to calculate electron density profiles at 30 °C, i.e., above the main transition. Examples of these profiles at 10, 20, and 30% hydration are shown in Figure 10. In all cases, the electron density distribution across the bilayer center is relatively shallow (Figure 10) and does not show a pronounced trough. From the location of the two electron-rich peaks at ± 15.5 –16 \AA , the bilayer thickness, d_{p-p} , is essentially constant at 31–32 \AA over the hydration range 10–40% of water (Figures 7B and 10). Over this hydration range, the water layer thickness d_w increases from 12.0 to 29.0 \AA (see Figure 7B). It is noticed that the lipid layer thickness, d_{p-p} , is slightly greater for the liquid-crystalline state (31–32 \AA) than for the gel state (29 \AA) whereas the water layer

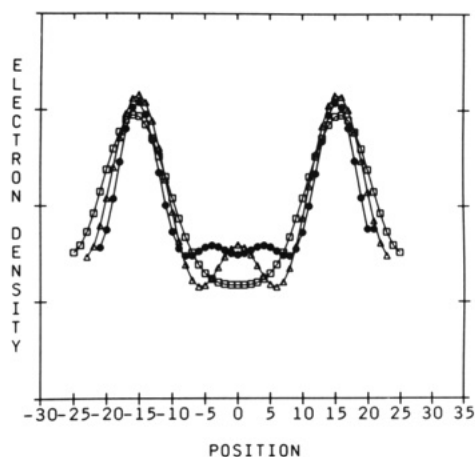


FIGURE 10: Electron density profiles of C(8):C(18)-PC at 30 °C for different hydrations: (●) 10% H₂O ($h = 1-4$); (Δ) 20% H₂O ($h = 1-3$); (□) 30% H₂O ($h = 1-3$). Assigned phases are --+--.

thickness, d_w , is almost the same for both phases, except at higher water concentrations.

Similar experiments were carried out with C(10):C(18)-PC. The X-ray diffraction pattern of C(10):C(18)-PC (at 10 wt % water) at low temperature (0 °C), shows multiple wide-angle reflections at 3.8, 4.1, 4.5, 4.7, 5.0, 5.4, 5.9, and 6.3 Å consistent with highly ordered, crystalline chain packing, whereas the low-angle region shows diffraction lines corresponding to two lamellar phases: one dominant phase with $d = 55.1$ Å (small arrows) and another phase with a smaller periodicity of 46.8 Å (large arrows) (Figure 11A). Above T_m , 30 °C, the wide-angle region consists of a diffuse band at 4.5 Å, and the low-angle region shows sharp reflections corresponding to a single lamellar phase with $d = 47.1$ Å (Figure 11B). At higher hydration (80% H₂O), at 0 °C, the wide-angle pattern shows sharp reflections at 3.8, 4.1, and 4.5 Å, and the low-angle diffraction pattern again displays the coexistence of the two phases with $d = 52.3$ Å (large arrows) and 62.5 Å (small arrows) (Figure 11C). At higher temperature (30 °C), a single lamellar phase is observed with $d = 61$ Å (data not shown). On cooling back to 0 °C (Figure 11D), again two phases are observed with a comparatively increased intensity of the 4.1-Å reflection and the lamellar series with $d = 52.3$ Å (large arrows, cf. Figure 11C,D). Comparison with the diffraction pattern of C(8):C(18)-PC (see Figure 6A,B) suggests that the phase with a smaller bilayer periodicity, $d = 52.3$ Å, and corresponding wide-angle reflection at 4.1 Å is an interdigitated gel phase, whereas the other phase with a larger bilayer periodicity, $d = 62.5$ Å, and wide-angle reflections at 4.5 and 3.8 Å is a bilayer phase with crystalline chain packing. This is consistent with the DSC data (Figure 3B) suggesting that after low-temperature incubation the crystalline bilayer phase predominates, whereas after cooling from the L_α phase the interdigitated gel phase predominates.

DISCUSSION

The calorimetric study of two series of mixed-chain PCs shows that the thermodynamic properties of both series do not change systematically as the chain length asymmetry is increased. The thermodynamic data plotted as a function of the chain length at the $sn-1$ and $sn-2$ positions show that for the C(18):C(n)-PC series, T_m decreases as the $sn-2$ chain decreases from 18 to 12 and then increases slightly for C(18):C(10)-PC followed by a large decrease for C(18):C(8)-PC. On further decreasing the chain length, T_m again increases. For the C(n):C(18)-PC series, T_m decreases sharply as the $sn-1$ chain

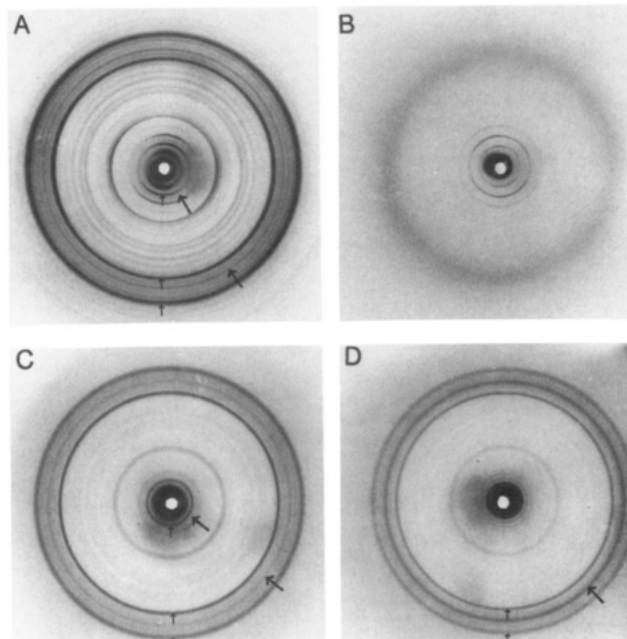


FIGURE 11: Representative X-ray diffraction patterns of hydrated C(10):C(18)-PC. (A) 10% H₂O at 0 °C after low-temperature incubation; (B) 10% H₂O at 30 °C; (C) 80% H₂O at 0 °C after low-temperature incubation; (D) 80% H₂O at 0 °C without low-temperature incubation.

length decreases from 18 to 10. For C(8):C(18)-PC, there is a small decrease of 2 °C followed by a large decrease for C(6):C(10)-PC. Thus, there is a small plateau on both sides of C(18):C(18)-PC suggestive of chain length dependent, structural changes. A similar trend is shown by the transition enthalpies and entropies. More specifically, the DSC data indicate a similarity in the thermotropic properties of the C(18):C(12)- and C(18):C(10)-PC compared to C(10):C(18)- and C(8):C(18)-PC. This led us to focus on C(8):C(18)-PC and C(10):C(18)-PC, in order to examine whether they exhibit similar structural behavior to that reported by Hui et al. (1984) and McIntosh et al. (1984) for C(18):C(12)-PC and C(18):C(10)-PC.

Our detailed calorimetric and X-ray diffraction studies of C(8):C(18)- and C(10):C(18)-PC demonstrate that the two PCs exhibit different behavior. The DSC scans of C(8):C(18)-PC show a sharp and symmetric chain melting transition. The bilayer phase formed at 0 °C (below the chain melting transition) is a stable phase and is essentially unchanged with the hydration or the thermal history of the sample since no crystalline phase was observed on prolonged incubation at low temperature (0, -10, or -12 °C). These results are in good agreement with the DSC measurements reported by Xu & Huang (1987). Similar thermal behavior is exhibited by C(18):C(10)-PC [see Mattai et al. (1987)].

Our X-ray diffraction data from the low-temperature phase of C(8):C(18)-PC, at 0 °C, show a lamellar gel phase at all hydrations. The sharp and symmetric wide-angle diffraction at 4.1 Å indicates that the hydrocarbon chains are not significantly tilted with respect to the bilayer normal and are packed in a hexagonal array similar to that described for other L_β gel phases (Tardieu et al., 1973). No major changes in chain-tilt with hydration are observed as indicated by the invariant shape and position of the 4.1-Å reflection at all hydrations studied. However, minor changes in chain tilt with increasing hydration, consistent with changes in the calculated area S (Figure 7) cannot be completely ruled out. This gel phase swells to a maximum at approximately 40% hydration

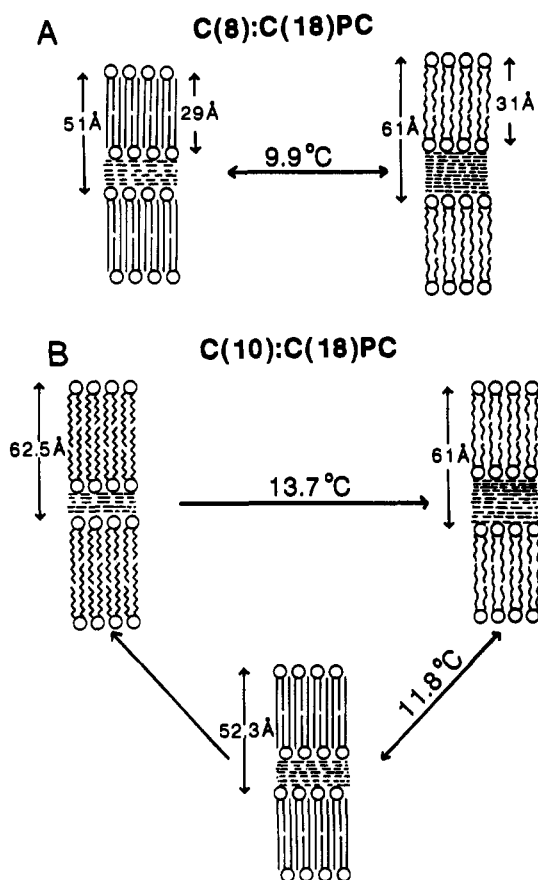


FIGURE 12: Schematic models and summary of the temperature-dependent structural changes exhibited by fully hydrated C(8):C(18)-PC (A) and C(10):C(18)-PC (B).

corresponding to approximately 24 molecules of water "bound" per molecule of C(8):C(18)-PC. The small values of both d_1 and d_{p-p} (29 Å), together with the central trough in the electron density profile, indicate that the hydrocarbon chains are interdigitated in a triple-chain manner (Figure 12A). The longer acyl chain at the *sn*-2 position extends across the entire bilayer width, whereas the shorter chain at the *sn*-1 position packs end-to-end with the short *sn*-1 chain of a PC molecule in the opposite bilayer leaflet, giving rise to the low electron density region in the center of the bilayer (see Figure 9). Moreover, the shape of the electron density profiles is similar to the electron density profiles of other mixed interdigitated bilayer systems, e.g., C(18):C(10)-PC (McIntosh et al., 1984). However, at 30 °C, d_{p-p} actually increases slightly to 31–32 Å, and the central trough is shallow, consistent with the two-chain arrangement where the long acyl chain of one PC molecule aligns against the short acyl chain of another PC molecule from the opposite monolayer (Figure 12A). It should be emphasized that both analyses show that the lipid thickness (d_1 or d_{p-p}) for the low-temperature gel phase is smaller than the lipid thickness for the liquid-crystalline L_α phase. Again, this is consistent with the mixed interdigitated bilayer model for C(8):C(18)-PC in the gel state. Using the Luzzati formalism, we have calculated the average area available to one C(8):C(18)-PC molecule in the gel state, at the lipid–water interface, to be 56.7–67.6 Å². The area per hydrocarbon chain, determined from the wide-angle reflection assuming hexagonal chain packing, gave a value of 19.5 Å². Clearly, there is sufficient area available to accommodate three hydrocarbon chains per head group, again consistent with an interdigitated three-chain bilayer model.

For C(10):C(18)-PC, the DSC measurements suggest the

formation of a bilayer phase with crystalline chain packing following incubation at low temperatures. Both the chain melting temperature and the transition enthalpy of the crystalline bilayer phase of this PC are higher than those of the gel phase (see Figure 3B), indicating that the crystalline bilayer phase is more stable than the metastable gel phase. The asymmetry in the endothermic transition on reheating is perhaps due to the coexistence of a small amount of the crystalline phase with the dominant gel phase (see Figure 3B, bottom). This is supported by the X-ray diffraction data for C(10):C(18)-PC at 0 °C (Figure 11A,C,D). Clearly, there are two phases existing simultaneously at $T < T_m$, one corresponding to a noninterdigitated bilayer crystalline state ($d = 62.5 \text{ \AA}$ at 80% H₂O) and the other to an interdigitated bilayer with a short lamellar repeat period, $d = 52.3 \text{ \AA}$ at 80% H₂O. Apparently, the conversion of the interdigitated L_β phase (formed on cooling) to the stable crystalline bilayer phase is inhibited at higher water content (cf. Figure 11A,C). A combination of the DSC and X-ray diffraction data of C(10):C(18)-PC provides a consistent picture of its thermotropic behavior and structural changes as shown in Figure 12B.

The structure and behavior of fully hydrated C(8):C(18)-PC and C(10):C(18)-PC are compared in Figure 12. C(8):C(18)-PC at $T < T_m$ shows a packing model in which there are three acyl chains per lipid head group. This model gives rise to a very stable gel phase which is independent of the hydration or low-temperature incubation of the sample. The transition from this stable state to liquid-crystalline state is a rapidly reversible process. This behavior is identical with that of C(18):C(10)-PC studied previously (Hui et al., 1984; McIntosh et al., 1984; Mattai et al., 1987). However, C(10):C(18)-PC at $T < T_m$ can form two types of bilayer phases; one, a regular two-chain bilayer; and the other, an interdigitated triple-chain bilayer. The relative amounts of the two phases present at low temperature depend on the thermal history of the sample, the kinetics of the interconversion, and the extent of hydration. This behavior is similar to that exhibited by C(18):C(12)-PC (Hui et al., 1984; Mattai et al., 1987). Apparently C(10):C(18)-PC lies at the border where on increasing the *sn*-1 chain length a regular two-hydrocarbon chain bilayer exists and lowering the chain length a triple-chain bilayer is formed.

Obviously, C(8):C(18)-PC behaves identically with C(18):C(10)-PC and not with its positional isomer C(18):C(8)-PC; similarly, C(10):C(18)-PC resembles C(18):C(12)-PC rather than its positional isomer C(18):C(10)-PC. The explanation of this pattern of behavior presumably lies in the molecular conformation of PC in the bilayers, most notably in the different conformation of the *sn*-1 (straight) and *sn*-2 (bent) chains due to the orientation of the glycerol moiety [see Hitchcock et al. (1974) and Hauser et al. (1981)].

ACKNOWLEDGMENTS

We thank Dr. J. Mattai for helpful discussions, D. Jackson for technical assistance, and Dr. D. Atkinson for valuable advice.

REFERENCES

- Barenholz, Y., & Thompson, T. E. (1980) *Biochim. Biophys. Acta* 604, 129–158.
- Boggs, J. M., & Mason, J. T. (1986) *Biochim. Biophys. Acta* 863, 231–242.
- Chapman, D., Williams, R. M., & Ladbroke, B. D. (1967) *Chem. Phys. Lipids* 1, 445–475.
- Chen, S. C., & Sturtevant, J. M. (1981) *Biochemistry* 20, 713–718.

- Gaber, B. P., & Peticolas, W. L. (1977) *Biochim. Biophys. Acta* 465, 260–274.
- Gupta, C. M., Radhakrishnan, R., & Khorana, H. G. (1977) *Proc. Natl. Acad. Sci. U.S.A.* 74, 4315–4319.
- Hauser, H., Pascher, I., Pearson, R. H., & Sundell, S. (1981) *Biochim. Biophys. Acta* 650, 21–51.
- Hitchcock, P. B., Mason, R., Thomas, K. M., & Shipley, G. G. (1974) *Proc. Natl. Acad. Sci. U.S.A.* 71, 3036–3040.
- Huang, C., & Mason, J. T. (1986) *Biochim. Biophys. Acta* 864, 423–470.
- Huang, C., Mason, J. T., & Levin, I. W. (1983) *Biochemistry* 22, 2775–2780.
- Hui, S. W., Mason, J. T., & Huang, C. (1984) *Biochemistry* 23, 5570–5577.
- Janiak, M. J., Small, D. M., & Shipley, G. G. (1976) *Biochemistry* 15, 4575–4580.
- Janiak, M. J., Small, D. M., & Shipley, G. G. (1979) *J. Biol. Chem.* 254, 6068–6078.
- King, G. I. (1971) Ph.D. Thesis, University of Michigan, University Microfilms, Ann Arbor, MI.
- King, G. I., & Worthington, C. R. (1971) *Phys. Lett.* 35A, 259–260.
- Luzzati, V. (1968) in *Biological Membranes* (Chapman, D., ed.) pp 71–123, Academic Press, London and New York.
- Mabrey, S., & Sturtevant, J. M. (1976) *Proc. Natl. Acad. Sci. U.S.A.* 73, 3862–3866.
- Mason, J. T., Huang, C., & Biltonen, R. L. (1981a) *Biochemistry* 20, 6086–6092.
- Mason, J. T., Broccoli, A. V., & Huang, C. (1981b) *Anal. Biochem.* 113, 96–101.
- Mattai, J., & Shipley, G. G. (1986) *Biochim. Biophys. Acta* 859, 257–265.
- Mattai, J., Sripada, P. K., & Shipley, G. G. (1987) *Biochemistry* 26, 3287–3297.
- McIntosh, T. J., Simon, S. A., Ellington, J. C., Jr., & Porter, N. A. (1984) *Biochemistry* 23, 4038–4044.
- Morrison, W. R., & Smith, L. M. (1964) *J. Lipid Res.* 5, 600–608.
- Nagle, J. F., & Wilkinson, D. A. (1978) *Biophys. J.* 23, 159–175.
- Ruocco, M. J., & Shipley, G. G. (1982a) *Biochim. Biophys. Acta* 684, 59–66.
- Ruocco, M. J., & Shipley, G. G. (1982b) *Biochim. Biophys. Acta* 691, 309–320.
- Sayre, D. (1952) *Acta Crystallogr.* 5, 843.
- Serrallach, E. N., de Haas, G. H., & Shipley, G. G. (1984) *Biochemistry* 23, 713–720.
- Shannon, C. E. (1949) *Proc. Inst. Radio. Eng. N.Y.* 37, 10–21.
- Stumpel, J., Nicksch, A., & Eibl, H. (1981) *Biochemistry* 20, 662–665.
- Stumpel, J., Eibl, H., & Nicksch, A. (1983) *Biochim. Biophys. Acta* 727, 246–254.
- Tardieu, A., Luzzati, V., & Reman, F. C. (1973) *J. Mol. Biol.* 75, 711–733.
- Torbet, J., & Wilkins, M. H. F. (1976) *J. Theor. Biol.* 62, 447–458.
- Worthington, C. R., & Blaurock, A. E. (1969) *Biophys. J.* 9, 970–990.
- Xu, H., & Huang, C. (1987) *Biochemistry* 26, 1036–1043.
- Yellin, N., & Levin, I. W. (1977) *Biochemistry* 16, 642–647.